Experimental Studies on Long-Wavelength Instability and Spiral Breakup in a Reaction-Diffusion System

Lu Qun Zhou and Qi Ouyang*

Department of Physics, Mesoscopic Physics Laboratory, Peking University, Beijing 100871, Peoples Republic of China

(Received 6 December 1999)

We investigate the behavior of spiral waves in a quasi-two-dimensional spatial open reactor using Belousov-Zhabotinsky reaction. The goal of this study is to answer two questions raised recently: Can a system sustain a stable long-wavelength modulated spiral? What causes the transition from spiral to defect-mediated turbulence? Our experimental results show that in a certain range of control parameters, a sustained long-wavelength modulated spiral is stable. The amplitude and the wavelength of modulations increase with the control parameter. As the latter is increased to across a threshold, defects are generated far away from the spiral center as a result of the neighboring two wave fronts being too close.

PACS numbers: 47.20.Lz, 47.27.Cn, 82.20.Mj

Transition from regular patterns to spatiotemporal chaos has received considerable attention, and is found in many systems of interest, such as fluid flows [1–4], cardiac tissue [5–7], populations of slime mold [8], and reaction-diffusion system [9–12]. Among them, spiral wave instability in a reaction-diffusion system is one of the most robust phenomena observed in experiments. With the control parameters varied, instability occurs so that spiral waves break up and the system undergoes a transition to a state of defect-mediated turbulence. Three different breakup scenarios are documented in experiments. In the first case, transition to spatiotemporal chaos occurs when a periodic external forcing is added and the ratio of the spiral-rotation period to that of the forcing is close to $3/2$ [11]; in the second case, spiral waves break near the spiral core due to a Doppler instability [12,13], when a Hopf bifurcation contributes to spiral core, making the latter meandering [14]; in the third case, spiral waves become unstable and break up far away from the core because of a long wavelength instability [10].

Spiral waves far away from the tip can be considered as planar wave trains in an oscillatory system. Near the onset of Hopf bifurcation, the system's variable can be written as a function of time t: $c = c_0 + A\exp(i\omega_c t) +$ c.c. In a ferroin catalyzed BZ reaction, c corresponds to the concentration of ferroin, ω_c is the Hopf frequency, and A is the complex amplitude of oscillations which obeys the complex Ginzburg-Laudau equation (CGLE) in one dimension:

$$\tau_0 \frac{\partial A}{\partial t} = \mu A + (g_1 + \mathrm{i}g_2)\frac{\partial^2 A}{\partial x^2} - \xi_0^2(d_1 + \mathrm{i}d_2)|A|^2 A, \tag{1}$$

where τ_0 and ξ_0 are, respectively, the characteristic time and the correlation length of the system. g_1, g_2, d_1, and d_2, are related to the diffusion coefficients and ensemble of reaction kinetics. Using τ_0 and ξ_0 as time and length units, after rescaling we have

$$\frac{\partial A}{\partial t} = A + (1 + \mathrm{i}\alpha)\frac{\partial^2 A}{\partial x^2} - (1 + \mathrm{i}\beta)|A|^2 A, \tag{2}$$

where $\alpha = d_2/d_1$ and $\beta = g_2/g_1$ are control parameters. Equation (2) has traveling plane wave solutions $A_0 = F\exp[\mathrm{i}(kx - \omega t)]$, where $F^2 = 1 - k^2$ and $\omega = \alpha k^2 + \beta(1 - k^2)$. They exist for $k^2 < 1$. The linear stability analyses [15,16] show that in the long wavelength limit, the complex growth rate λ as a function of the wave number of inhomogeneous perturbations p satisfies

$$\lambda(p) = iv_g p - D_{\|}p^2 + O(p^3), \tag{3}$$

where $v_g = 2(\beta - \alpha)k$ and $D_{\|} = 1 + \alpha\beta - 2k^2(1 + \beta^2)/(1 - k^2)$. When $D_{\|} < 0$, the so-called Eckhaus instability occurs. This instability is a long-wavelength instability and has a convective nature.

Further nonlinear analyses reveal that Eckhaus instability does not directly lead to a spiral wave breakup, generating defect-mediated turbulence. A stable long wavelength modulated solution is expected [1]. Recently, Tobias and Knobloch [17] pointed out that the spiral wave breakup is due to the appearance of an unstable global mode that asymptotes to the absolute instability, and both the modulation waves and the resulting instability move in from the boundary. However, the numerical simulation conducted by Bär *et al.* [18] on a reaction-diffusion model indicates that, for oscillatory conditions, the convective variant of Eckhaus instability exists, and the breakup does not begin to occur from the boundary. This result is consistent with the predictions of Janiaud *et al.* [1,15].

In this Letter, we investigate the long-wavelength instability and breakup of spiral waves in experiments with a quasi-two-dimensional BZ reaction. We observe that local perturbations can saturate in time after the instability occurs. As a result, sustained long-wavelength modulated spiral waves will appear, and the pattern is stable in the finite size of the reactor. The amplitude and the wavelength of modulations increase with the control parameter. As the

 0031-9007/00/85(8)/1650(4)$15.00

latter is increased to across a threshold, defects are generated far away from the center, as a result of the neighboring two wave fronts being too close.

The experimental setup and chemical compositions are the same as that described in Ref. [12], except we use higher concentrations of sodium bromate and malonic acid (see caption of Fig. 1). As in the previous work [10,12], the initial condition is chosen such that only one spiral tip is located in the center of reaction medium. The concentration of sulfuric acid in compartment B ($[H_2SO_4]_B$) is chosen as the control parameter. Enough time (about an hour) is allowed between changes of the control parameter so that the system can relax to its new asymptotic state. At low $[H_2SO_4]_B$ (0.63 M), the spiral state is stable; a spiral simply rotates and its waves travel outward, as shown in Fig. 1(a). Because the reaction medium is much larger than the spiral wavelength (aspect ratio $\approx$50), the influence of the boundary is not important.

As $[H_2SO_4]_B$ is increased to across a critical value (0.72 M), the long-wavelength instability settles in. As a result, apparent spatially modulated waves emerge so that the distance between successive wave fronts (the local wavelength) varies spatially; see Figs. 1(b) and 1(c). The optical intensity $I(x)$ of the spiral waves along the distance from the spiral core is shown in Fig. 2(a). It has clear amplitude and phase modulations. Figure 2(b) shows the local wavelength variation, which is obtained by wavelet technique. One observes that the phase modulation is spatially periodic, and it goes in phase with amplitude modulation. This is consistent with the observation in Ref. [1]. The spatial Fourier spectrum, as shown in Fig. 2(c), exhibits two independent peaks at k_c and k_m, respectively, corresponding to the carrier and the modulational wave number [proportional to k and p in Eq. (3)]. The ratio of the two wave numbers is 5.33, thus the instability is of a long-wavelength type. Peaks of combinations of k_c and k_m ($k_c \pm k_m$, $k_c \pm 2k_m$) are also shown in the spectrum. They show asymmetry in the power of the sidebands. Between $[H_2SO_4]_B = 0.72 - 0.94$ M, no additional defects appear and the long-wavelength modulated spiral is sustained in the finite reaction medium.

We measure the periods, the wavelengths, and the traveling speeds of the long-wavelength modulation and their carrier waves as a function of the control parameter [19]. The results are presented in Fig. 3. Near the onset of the long-wavelength instability, the period of the long-wavelength modulation decreases with the increase of the control parameter [Fig. 3(a)], while the corresponding wavelength varies little [Fig. 3(c)]. However, when $[H_2SO_4]_B$ passes across a value (0.80 M), the period of the modulation waves attains to a minimum value and then begins to increase [Fig. 3(a)], at the same time the modulation wavelength also increases with the control parameter [Fig. 3(c)]. Meanwhile, the period of the carrier waves always decreases, but the rate of decrease changes at the turning point [Fig. 3(b)]. Figure 3(e) presents the phase velocities V_m and V_c as a function of the control parameter. Although there is a turning point in the periods of modulation and carrier waves [Figs. 3(a)

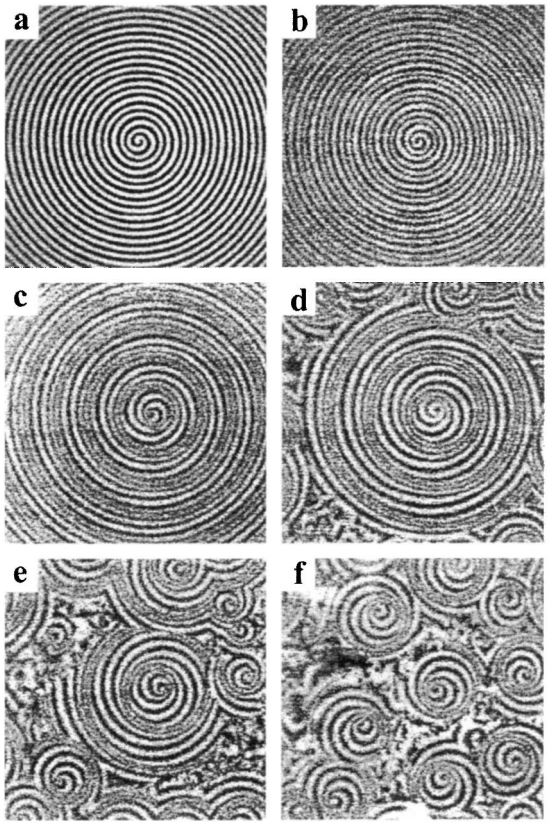

FIG. 1. The snapshots of long-wavelength modulated spirals and defect-mediated turbulence. $[H_2SO_4]_B$ (in M): (a) 0.63, simple periodic spiral; (b) 0.765, onset of the long-wavelength instability; (c) 0.90, full developed modulated spirals; (d) 0.94, and (e) 0.95, onset and beyond of defect-mediated turbulence; (f) 0.97, a state of compact laminar disks. Other control parameters are kept fixed: $[MA]_A = 0.4$ M, $[KBr]_B = 30$ mM, $[NaBrO_3]_{A(B)} = 0.6$ M, [ferroin]$_B = 1.0$ mM, and temperature 25 ± 0.5 °C. The images shown are 13.3×13.3 mm.

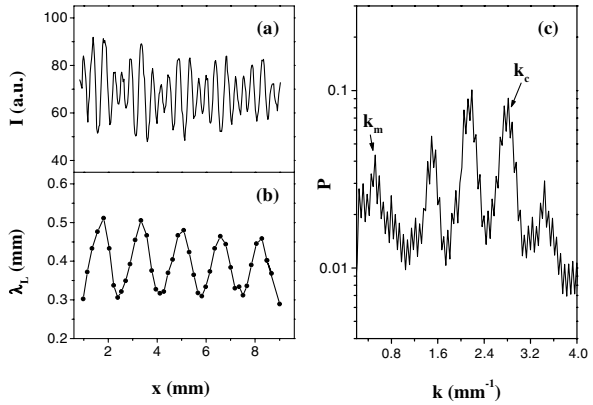

FIG. 2. Measurements of the long-wavelength instability in Fig. 1(c). (a) Optical intensity of spiral waves as a function of the distance from the spiral core. (b) The variation of local wavelength with the distance. (c) The spatial power spectrum.

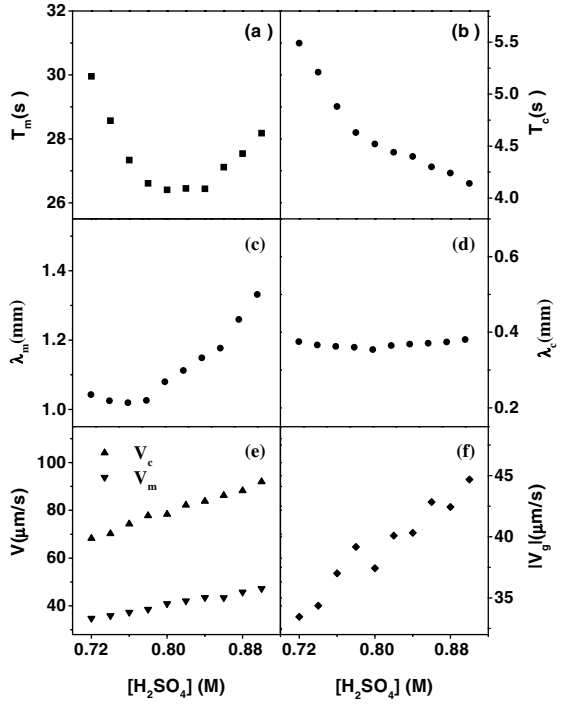

FIG. 3. The periods [(a), (b)], the wavelengths [(c), (d)], and the phase velocities [(e)] of the modulation and carrier waves measured as a function of $[H_2SO_4]_B$ at onset and beyond the long-wavelength instability. The subscripts m and c denote modulation and carrier waves, respectively. (f) The absolute value of convective velocity $|V_g|$.

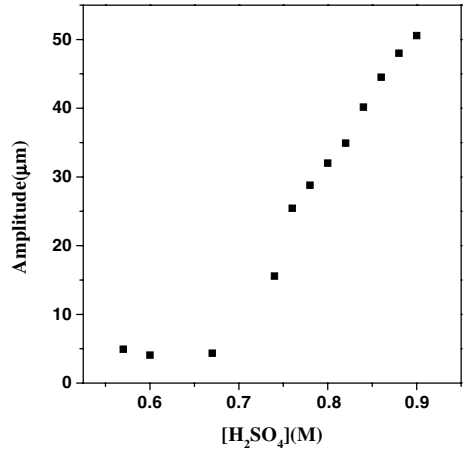

FIG. 4. The amplitude of phase modulation as a function of the control parameter. The nonzero values before the onset ($[H_2SO_4]_B = 0.72$ M) reflect the error bars. Other parameters are fixed as in Fig. 1.

and 3(b)], the increase rate of the phase velocities seems to be constant [Fig. 3(e)]. One notices that the carrier wave propagates out faster than the modulation waves, so that the convective velocity relative to the carrier waves $V_g (= V_m - V_c)$ points to the spiral center. In Fig. 3(f), one observes that the convective velocities become larger with the increase of control parameter. From the above results, the onset of the long-wavelength instability is possibly due to Eckhaus instability.

Figure 4 presents the bifurcation diagram of the long-wavelength instability. The amplitude of the phase modulation is obtained by measuring local spiral wavelength, then calculating half of the difference between maximum and minimum values. One observes in Fig. 4 that the amplitude of the modulation increases with the control parameter. However, because of lacking data near the onset and a large error bar, we do not know if the curve obeys the square root law predicted by Janiaud *et al.* [1].

As the control parameter is increased across another threshold (0.94 M), defects are continuously generated; see Figs. 1(d), 1(e), and 1(f). The spiral breakup takes place far away from the center, and there exists a disk of laminar core of the spiral where turbulence cannot invade. Thus the system is separated into two different regimes: ordered spiral waves inside the core and defect-mediated turbulence outside of the core. The size of laminar core decreases as the control parameter increases. However, in the turbulent sea there are some of the defects having chances to develop into spirals, generating many laminar cores of ordered spirals. The sizes of the laminar cores tend to be equal, and the cores tend to form a compact pattern; see Fig. 1(f). At last, when $[H_2SO_4]$ is above 1.0 M, the turbulence state will invade the whole space, which is not shown here.

The coexistence of several stable laminar core regions in Fig. 1(f) hints that defects are not generated from the boundary. Where and how do these defects first emerge? To answer this question, we conduct the following experiment: $[H_2SO_4]_B$ is changed so that the system jumps from a state of stable modulated spiral directly to a state of full turbulence. Observation of transient behavior of the system will give us the information of how the instability develops and the defects are generated as time goes by. This process is presented in Fig. 5. At the beginning, we have a long-wavelength modulated spiral [Fig. 5(a)]. After changing the control parameter, one observes that the amplitude and the wavelength of modulation waves increase as they spiral out from the spiral center, as shown in Fig. 5(b). As a result, locally the long wavelengths become longer and the short ones become narrower. When some local wavelengths are too small, the wave fronts become unstable. This leads to the wave fronts' breakup and the emergence of defects, as shown in Figs. 5(c) and 5(d). It is clear that the phase modulation generated from spiral center is responsible for the spiral breakup. Gradually, more and more defects appear. When $t = 419$ s, only a small spiral core remains stable, out of which the defects-mediated turbulence dominates, as shown in Fig. 5(e). At last, the turbulence almost invades the whole space; see Fig. 5(f).

Our experiment shows that a local modulation saturates in time for a given control parameter; see Fig. 1(b) and 1(c). However, due to the finite reactor size, we do not know whether the amplitude of modulation can be saturated as a function of space, or it is just a long-lived

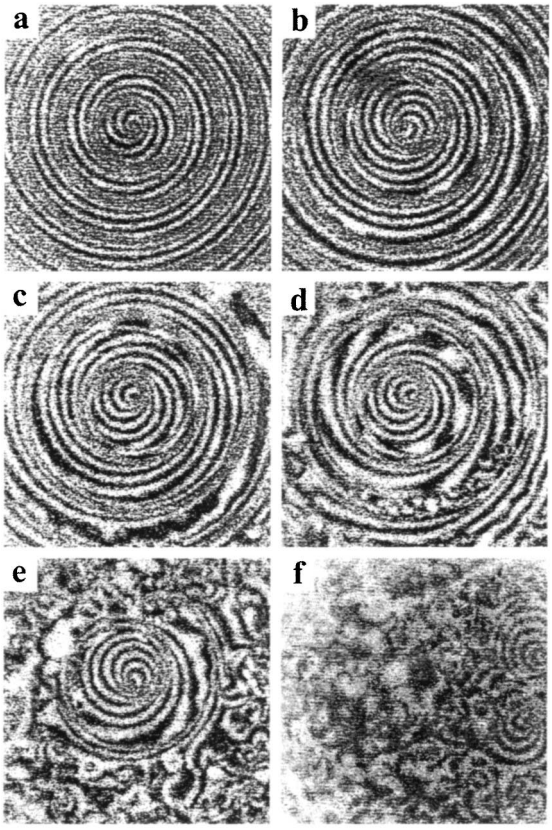

FIG. 5. The long-wavelength instability development as a function of time when $[H_2SO_4]_B$ is varied from 0.90 M directly to 1.05 M: (a) 0 s, (b) 239 s, (c) 272 s, (d) 334 s, (e) 419 s, and (f) 1985 s. Other parameters are the same as in Fig. 1.

transient. Indirect experimental evidence shows that the modulations are long-lived transient rather than stable. In the case of Fig. 1(c), if we move the spiral center to the upright corner of the reactor, we find that spiral waves break up at the down-left corner. This happens because the distance that allows a modulation to propagate in the observable area is almost doubled, so that the amplitude of modulation has space to increase to a lever that breaks spiral waves.

Several comments are in order. (i) Hynne *et al.* [20] measured the values of α and β in Eq. (2) for cerium catalyzed BZ reaction, and found they are -1.4 and 0.6, respectively. If we assume these values in our system, we have $v_g > 0$ [see Eq. (3)], which means that the convective velocity relative to the carrier waves points to the direction of the spiral center. Our observations in Fig. 3(e) agree with this result. However, since there are multiple gradients of concentrations across the reaction medium, we don't know the chemical compositions in the patterned layer, thus cannot deduce the values of α and β using the method introduced by Hynne *et al.* (ii) Although CGLE is a good model, it cannot fully describe traveling waves in BZ reaction. Chemical waves are dictated by a dispersion relation, which states that there exists a minimum wavelength, beyond which waves become unstable and break. We believe that this is what happened in the case of Fig. 5. (iii) It seems that there exist two types of dynamical behavior of the modulation waves. In one type, the modulation period decreases with the control parameter; in the other type, it increases with the control parameter, as shown in Figs. 3(a) and 3(b). We do not have a satisfactory explanation for this phenomenon at present.

We thank H. L. Swinney for providing us porous class disks and comments on our manuscript. This work is supported by the Chinese Natural Science Foundation.

*Electronic address: qi@mail.phy.pku.edu.cn

[1] B. Janiaud *et al.,* Physica (Amsterdam) **55D**, 269 (1992).
[2] R. E. Ecke, Y. Hu, R. Mainieri, and G. Ahlers, Science **269**, 1704 (1995).
[3] B. B. Plapp, D. A. Egolf, E. Bodenschatz, and W. Pesch, Phys. Rev. Lett. **81**, 5334 (1998).
[4] N. Mukolobwiez, A. Chiffaudel, and F. Daviaud, Phys. Rev. Lett. **80**, 4661 (1998).
[5] J. M. Dadivenko, A. V. Pertsov, R. Salomonsz, W. Baxter, and J. Jalife, Nature (London) **355**, 349 (1992).
[6] A. T. Winfree, Science **266**, 1003 (1994).
[7] F. X. Witkowski *et al.,* Nature (London) **392**, 78 (1998).
[8] K. J. Lee, E. C. Cox, and R. E. Goldstein, Phys. Rev. Lett. **76**, 1174 (1996).
[9] Q. Ouyang and H. L. Swinney, Chaos **1**, 411 (1991).
[10] Q. Ouyang and J. M. Flesselles, Nature (London) **379**, 143 (1996).
[11] A. Belmonte, J.-M. Flesselles, and Q. Ouyang, Europhys. Lett. **35**, 665 (1996).
[12] Q. Ouyang, H. L. Swinney, and G. Li, Phys. Rev. Lett. **84**, 1047 (2000).
[13] M. Bär *et al.,* Chaos **4**, 499 (1994).
[14] D. Barkley, Phys. Rev. Lett. **68**, 2090 (1992).
[15] I. S. Aranson, L. Aranson, L. Kramer, and A. Weber, Phys. Rev. A **46**, R2992 (1992).
[16] L. Kramer, F. Hynne, P. Graae Sørenson, and D. Walgraef, Chaos **4**, 443 (1994).
[17] S. M. Tobias and E. Knobloch, Phys. Rev. Lett. **80**, 4811 (1998); S. M. Tobias, M. R. E. Proctor, and E. Knobloch, Physica (Amsterdam) **113D**, 43 (1998).
[18] M. Bär and M. Or-Guil, Phys. Rev. Lett. **82**, 1160 (1999).
[19] The average periods of the modulations T_m and the carrier waves T_c are measured by counting the number of wave fronts passing over a fixed point far from the spiral center in unit time. The wavelengths of modulation λ_m and carrier waves λ_c are measured directly from image and with Fourier transform. The phase velocities of modulation and carrier waves can thus be calculated: $V_m = \lambda_m/T_m$, $V_c = \lambda_c/T_c$.
[20] F. Hynne, P. G. Sørenson, and T. Møller, J. Chem. Phys. **98**, 219 (1993).